ResearchGate

See discussions, stats, and author profiles for this publication at: https://www.researchgate.net/publication/228096901

Electrochemical Characterization of Shape-Controlled Pt Nanoparticles in Different Supporting Electrolytes

ARTICLE *in* ACS CATALYSIS · MAY 2012

Impact Factor: 9.31 · DOI: 10.1021/cs200681x

CITATIONS
63

READS
32

5 AUTHORS, INCLUDING:

Rosa M. Arán Ais
University of Alicante
13 PUBLICATIONS **128** CITATIONS
SEE PROFILE

J.M. Feliu
University of Alicante
488 PUBLICATIONS **11,593** CITATIONS
SEE PROFILE

Available from: Rosa M. Arán Ais
Retrieved on: 22 January 2016

ACS Catalysis

Research Article

pubs.acs.org/acscatalysis

Electrochemical Characterization of Shape-Controlled Pt Nanoparticles in Different Supporting Electrolytes

Francisco J. Vidal-Iglesias, Rosa M. Arán-Ais, José Solla-Gullón, Enrique Herrero,* and Juan M. Feliu*

Instituto de Electroquímica, Universidad de Alicante, Apartado 99, 03080 Alicante, Spain

Supporting Information

ABSTRACT: The voltammetric profile of preferentially shaped platinum nanoparticles has been used to analyze the different sites present on the surface. For the first time, this analysis has been made in NaOH solutions and revisited in sulfuric and perchloric acid media. The comparison with the voltammetric profiles of the model surfaces, that is, single-crystal electrodes, allows assigning the different signals appearing in the voltammograms of the nanoparticle to specific sites on the surface. A good correlation between the shape of the nanoparticle determined by TEM and the voltammetric profile is obtained. For the nanoparticles characterized in alkaline media, the adsorbed species on the surface have been characterized, and three major regions can be identified. Below 0.2 V, the major contribution is due to hydrogen adsorption, whereas above 0.6 V, adsorbed OH is the main species on the surface. Between those values, the signals are due to the competitive adsorption/desorption process of OH/H. New criteria for determining the active area in NaOH solutions has been proposed. In this medium, the total charge density measured between 0.06 and 0.90 V stands for 390 μC cm^{-2}. The areas measured are in perfect agreement with those measured in acid media. Once the nanoparticles have been characterized, the behavior of the nanoparticles toward CO oxidation is analyzed and compared with that observed for single-crystal electrodes.

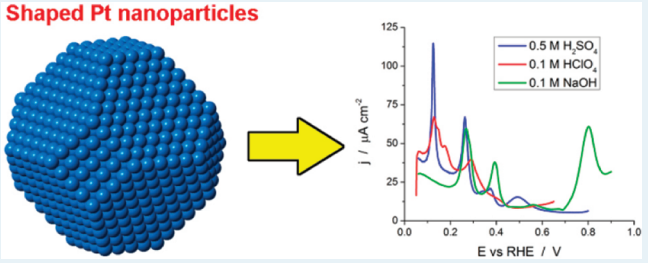

KEYWORDS: *platinum, nanoparticles characterization, alkaline media, CO oxidation*

INTRODUCTION

It is well-established that most of the electrocatalytic reactions of interest are structure-sensitive. This effect has been well documented by using single-crystal electrodes. In some cases, such as hydrogen oxidation or oxygen reduction, the reactivity of the single-crystal electrodes is similar, albeit some reactivity differences (measured current density at constant potential) can be observed.[1−3] These differences are more significant for the oxidation of potential organic fuels or for nitrogen-containing compounds.[4,5] In some particular cases, the reaction only takes place on a particular type of surface site.

For practical purposes, nanoparticle electrocatalysts dispersed on a suitable support are used. Because the reaction takes place on the surface sites, the surface structure of the nanoparticle will strongly control their reactivity. In recent years, the synthesis of shape-controlled Pt nanoparticles has been widely explored, with the main objective of obtaining more efficient catalysts.[6−9] Thus, it has been clearly shown that the reactivity and selectivity of the Pt nanoparticles can be modulated by controlling the morphology because the surface of the nanoparticles may contain very different reactive surface sites, depending on their shape.[7,10] In addition, these shape-controlled nanoparticles are ideal to understand the reactivity of practical electrodes, since they provide the missing link with the model surfaces, that is, the single-crystal electrodes. However, in most of the cases, the preparation of shape-controlled Pt nanoparticles requires the use of surface-stabilizing agents. Consequently, once the nanoparticles are synthesized, these stabilizing agents must be completely removed from the surface of the nanoparticles because, as previously stated, chemical or electrochemical reactions can be only understood on "clean" surfaces.

Obtaining reproducible measurements requires comparison between data on clean surfaces, because "contaminated" surfaces have unknown composition. Reproducibility is a key factor in science; that is, progress in the understanding of surface reactivity requires standard procedures to be fulfilled on the different laboratories. However, one question arises from this requirement: how should surface cleaning be evaluated? Fortunately, after more than 30 years of working with Pt in electrocatalysis, the level of cleanliness of the Pt surfaces can be readily evaluated by simply visualizing the so-called hydrogen adsorption desorption region.[11] Thus, the peak position, definition (sharpness), and the reversibility of the adsorption states in the so-called hydrogen and anion adsorption region can be employed as probes to estimate the surface cleanliness of the Pt nanoparticles, an imperative prerequisite for a correct surface characterization and further electrocatalytic evaluation.

Special Issue: Electrocatalysis

Received: December 22, 2011
Revised: March 19, 2012
Published: April 16, 2012

 © 2012 American Chemical Society dx.doi.org/10.1021/cs200681x | *ACS Catal.* 2012, 2, 901−910

Consequently, the criteria developed for validating single-crystal experiments should be also considered when the reactivity of nanoparticles is examined, which would allow gaining a comprehensive understanding of their intrinsic catalytic or electrocatalytic properties.

Interestingly, this hydrogen and anion adsorption region can also be used as probe reactions to define the properties of the surface. Two main reasons justify the use of this region for this purpose. First, the overall adsorption charge is directly proportional to the number of surface atoms and, thus, can be used to calculate the real surface area. Second, it is well-established that the orientation, the type of ordered domains, and the density of step sites of a Pt single-crystal plane, including basal, stepped, and kinked surfaces, could be readily characterized by using its voltammogram in the so-called hydrogen adsorption/desorption region.[12−16] Consequently, in the case of the shape-controlled Pt nanoparticles, the distribution of the charge among the different voltammetric peaks gives a first estimation of the presence of the different surface sites on the whole surface.[12,17] In addition, the characteristic response of the surface sites present at the nanoparticles can be analyzed by simple comparison with model single-crystal stepped surface electrodes, which consist of a regular succession of terraces with a given symmetry separated by monoatomic steps with a different, but controlled, symmetry. By changing the terrace width and the symmetry of the step, the contributions of the different domains can be analyzed and linked to the results of the real surfaces. An additional advantage is that all these measurements can be performed in solution, that is, the environment in which electrochemical reactions occur.

In this paper, we report and discuss the electrochemical response of some representative shape-controlled Pt nanoparticles in the so-called hydrogen adsorption/desorption region for different electrolytes. For the first time, this analysis is made in NaOH solution and revisited for H_2SO_4 and $HClO_4$ solutions. The results obtained will be correlated with those coming from model single-crystal Pt surfaces. In addition, a new criterion for determining the active surface area in NaOH is presented on the basis of the analysis of the electrochemical response of the different Pt basal planes and some stepped and kink surfaces obtained in the same experimental conditions as those employed in the case of the different nanoparticles as well as comparison with the active surface area of the nanoparticles determined in the other supporting electrolytes (H_2SO_4 and $HClO_4$). A correct determination of the active surface area is a question of paramount importance in electrocatalyis because it allows proper measurement of the intrinsic electrocatalytic properties of the system under study. We also report new insights into the CO stripping oxidation on the different shape-controlled Pt nanoparticles in this alkaline medium. These new results will be discussed in terms of CO electrooxidation on well-defined, stepped Pt single crystals, which has been recently studied in detail.[18−22]

EXPERIMENTAL SECTION

Synthesis and Cleaning of the Pt Nanoparticles. In this work, four types of Pt nanoparticles were prepared. Comprehensive experimental details on the synthesis are given in the Supporting Information. In brief, Pt nanoparticles with a preferential spherical shape ($PtNP_{sphe}$) were synthesized by reducing H_2PtCl_6 with sodium borohydride using a water-in-oil (w/o) microemulsion.[23−26] The other three types of nanoparticles (with a preferential cubic shape ($PtNP_{cubic}$), with a preferential octahedral tetrahedral shape ($PtNP_{tetra}$), and with a preferential octahedral and tetrahedral truncated shape ($PtNP_{trunc}$)) were synthesized with a colloidal method using sodium polyacrylate (PA, M_w = 2100) as capping agent, K_2PtCl_4 or H_2PtCl_6 as metallic precursor, and H_2 as reducing agent.[25,27,28]

Cleaning Process for the Shape-Controlled Pt Nanoparticles. After complete reduction (12−14 h), the shape-controlled Pt NPs were cleaned with a strong, basic, aqueous solution, followed by several water washes to finally achieve a water suspension with clean Pt nanoparticles. For the present experimental conditions (100 mL of solution), two NaOH pellets (≈0.2 g) are added to the colloidal suspension containing the shape-controlled Pt nanoparticles. Once NaOH is dissolved, the sample is left to stand until complete precipitation. After solvent removal, the nanoparticles were washed 3−4 times with ultrapure water. The previously described cleaning procedures should be considered valid exclusively for the current synthetic methodologies and should not be taken as a general cleaning method. For instance, we have tried to employ the same cleaning methodology for shape-controlled Pt nanoparticles synthesized with PVP, which is one of the most widely employed stabilizing agents, with negative results.

Characterization of Pt Nanoparticles by TEM. Transmission electron microscopy (TEM) and high resolution transmission electron microscopy (HRTEM) have been employed to investigate the shape of the nanoparticles at the atomic scale. TEM experiments were performed with a JEOL, JEM 2010 microscope working at 200 kV, whereas HRTEM experiments have been carried out on a JEOL 3010 microscope (LaB6, Cs = 1.1 mm) operated at 300 kV, providing a point-to-point resolution of 0.19 nm. The sample was obtained by placing a drop of the dispersed solution onto a Formvar-covered copper grid and evaporating it in air at room temperature. For each sample, usually more than 200 particles from different parts of the grid were used to estimate the mean diameter and size distribution of the nanoparticles. Despite that the micrographs provide only a 2D projection of these particles, they clearly evidence that the nanoparticles crystallize with different shapes.

Platinum Single-Crystal Electrodes. Platinum single crystals were oriented, cut, and polished from small single-crystal beads (∼2.5 mm diameter) by a procedure described previously.[29] The electrodes were flame-annealed and cooled in a H_2 + Ar atmosphere in the usual way.[30] It has been shown that this treatment leads to well-defined surfaces.[31] A single-crystal platinum bead obtained by fusion of a Pt wire was used as a polycrystalline surface having a uniform distribution of all surface sites (Pt poly). A detailed description of the single-crystal surfaces is given in the Supporting Information (Table S1).

Electrochemical Characterization. The electrochemical characterization of the samples, both single-crystal surfaces and Pt nanoparticles, was performed in a three-electrode electrochemical cell. The electrode potential was controlled using a PGSTAT30 AUTOLAB system. The counter electrode was a gold wire. Potentials were measured against a reversible hydrogen electrode (RHE) connected to the cell through a Luggin capillary. For the Pt nanoparticles, a droplet ranging from 1 to 3 μL of the solution containing the nanoparticles was deposited on a hemispherical polycrystalline gold substrate and

dx.doi.org/10.1021/cs200681x | ACS Catal. 2012, 2, 901−910

dried under an Ar atmosphere. Before each experiment, the gold collector was mechanically polished with alumina and rinsed with ultrapure water to eliminate the nanoparticles from previous experiments. To perform the adsorbed CO oxidation experiments, CO(g) was bubbled through the electrolyte at an admission potential of 0.05 V until complete blockage of the surface was reached, which was monitored by cycling the electrode between 0.05 and 0.35 V. After that, CO was removed from the solution by bubbling Ar for at least 20 min. CO-stripping voltammograms were registered at 20 mV s^{-1} to oxidize the CO molecules adsorbed on the surface in a single sweep. The supporting electrolytes, 0.5 M H_2SO_4 and 0.1 M $HClO_4$, were prepared from suprapur quality (Merck) and 0.1 M NaOH solutions from p.a. quality (Merck) NaOH pellets. Solutions were prepared using Millipore Milli-Q water. Oxygen was eliminated by bubbling Ar (Air Liquide N50) for 20 min.

The determination of the active surface area of the Pt nanoparticles is a question of paramount importance in electrocatalyis because it allows properly determining the intrinsic electrocatalytic properties of the system under study. In the present work, the active surface area of the different Pt nanoparticles was determined in H_2SO_4 and in $HClO_4$ by the charge involved in the so-called hydrogen UPD region assuming 230 and 200 μC cm^{-2}, respectively, for the total charge after the subtraction of the double layer charging contribution, as previously discussed.[10] However, in the case of the alkaline medium, the determination of the active surface area is not straightforward and will be studied in more detail in the present manuscript.

RESULTS

Voltammetric Characterization of the Nanoparticles. $PtNP_{sphe}$, $PtNP_{cubic}$, $PtNP_{tetra}$, and $PtNP_{trunc}$ nanoparticles with particle sizes of 4.5 ± 0.8, 8.2 ± 1.6, 8.5 ± 1.4, and 9.7 ± 1.6 nm, respectively, were successfully obtained after synthetic procedures (see Supporting Information Figures S1−S3 for some representative TEM and HRTEM images of the Pt nanoparticles as well as their particle size histograms). In terms of surface structure, these samples can be assigned to polyoriented, (100), (111), and (111)−(100) preferentially oriented Pt nanoparticles, respectively.

Figure 1 shows the characteristic voltammetric profiles of the different Pt nanoparticles in 0.5 M H_2SO_4 after effective cleaning of their surfaces. The sharpness, good definition, and the symmetry of the adsorption states in all samples are clear evidence of the effective surface cleanliness. The analysis of the characteristic voltammetric features obtained in this medium was already discussed in detail in a previous contribution.[24] In summary, the main voltammetric features are (i) the peak at 0.125 V, which is related to (110)-type sites; (ii) the peak at 0.27 V, which contains two contributions from (100) step sites on (111) terraces and the sites close to the steps on the (100) terraces; (iii) the signals at 0.35−0.37 V attributed to (100) bidimensional terraces; and (iv) the signals at 0.5 V, related to the bidimensionally ordered (111) terraces. All these voltammetric profiles perfectly correlate with those obtained with Pt single-crystal electrodes (Supporting Information Figure S4). In this way, this simple electrochemical experiment can give us a first estimation of the presence of the different surface sites on the whole surface as well as evidence of the surface cleanliness.

Interestingly, all these states are observed in all Pt nanoparticles, but to a different extent, which reflects their

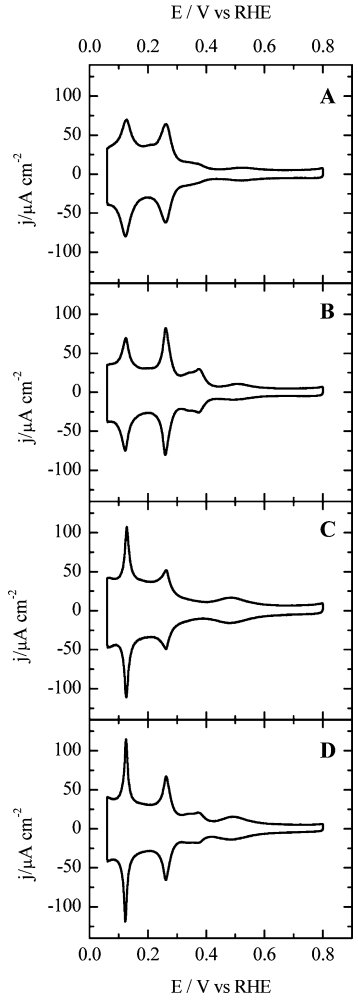

Figure 1. Voltammograms corresponding to (A) $PtNP_{sphe}$, (B) $PtNP_{cubic}$, (C) $PtNP_{tetra}$, and (D) $PtNP_{trunc}$ in 0.5 M H_2SO_4. Scan rate, 50 mV s^{-1}.

specific surface structure composition, in agreement with that suggested by the TEM measurements. In addition, surface probes sensitive to specific sites, such as Bi,[24,32,33] Ge,[24,34,35] or Te[24,36] adsorption and the deconvolution of the voltammetric profiles,[24] allow quantifying the relative number of sites present on the surface of the nanoparticle (see Supporting Information Table S2). These values are in very good agreement with the preferential shape determined from the TEM images. Thus, the voltammetric profile of $PtNP_{cubic}$ exhibits the largest contributions at 0.35−0.37 V assigned to the (100) ordered domains, whereas the (111) nanoparticles have the highest currents in the region corresponding to the (111) domains. In addition, it is worth noting that despite the size and shape dispersion of the samples and the voltammetric profile of each particular sample that reflects their surface structure, it is always the same for different aliquots of the sample in independent experiments. Consequently, their voltammetric profile can be used as a fingerprint of their specific surface structure.

Switching to $HClO_4$, and although it is known that the adsorption desorption peaks are not as well resolved in this electrolyte as in sulfuric acid, different voltammetric profiles can also be obtained in this medium from the distinct shape of the nanoparticles. In addition, it should be highlighted that the absence of specific anion adsorption causes the different adsorption states to spread in a wider potential range; that is,

dx.doi.org/10.1021/cs200681x | ACS Catal. 2012, 2, 901−910

the peaks become wider. This broader profile makes it more difficult to identify by simple inspection that the nanoparticle surfaces are clean, unlike the data obtained in sulfuric acid. Figure 2 shows the voltammograms obtained for the different

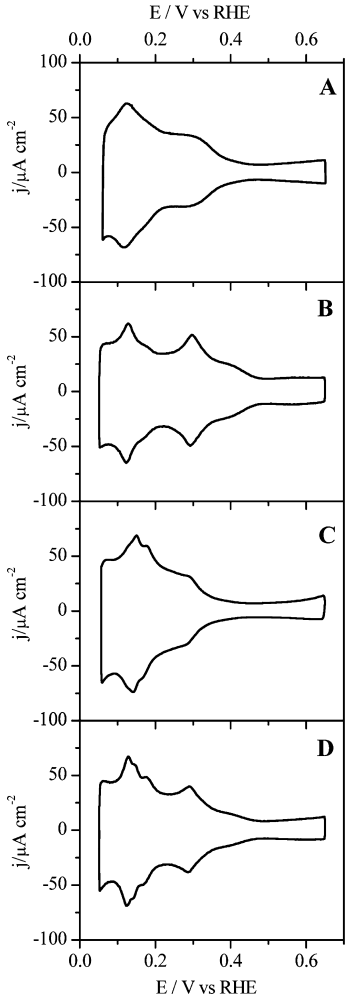

Figure 2. Voltammograms corresponding to (A) $PtNP_{sphe}$, (B) $PtNP_{cubic}$, (C) $PtNP_{tetra}$, and (D) $PtNP_{trunc}$ in 0.1 M $HClO_4$. Scan rate, 50 mV s^{-1}.

Pt nanoparticles. By comparison with those obtained with Pt single-crystal electrodes (Figure 3), it is possible to identify the main voltammetric features in this electrolyte. In detail, the contributions in the range between 0.4 and 0.6 V can be clearly related to the presence of (100) sites due to OH adsorption on the (100) well-ordered domains, as proposed for the single-crystal electrodes with this orientation.[37−39] Thus, the voltammograms of the $PtNP_{cubic}$ and also that of the $PtNP_{trunc}$, although that to a lesser extent, show a significant broad contribution in this region, in agreement with their preferential surface orientation as well as the results obtained in sulfuric media. This contribution is absent in the $PtNP_{tetra}$, which have a very low amount of well ordered (100) domains. On the other hand, the contributions in the range between 0.09 and 0.22 V can be attributed to (110) sites. Interestingly, a clear splitting in at least three different contributions, not detected in sulfuric acid, can be observed. Similar behavior has been seen in the voltammetry of Pt(110) single-crystal electrodes and its vicinal surfaces in perchloric acid and points out the complexity of this

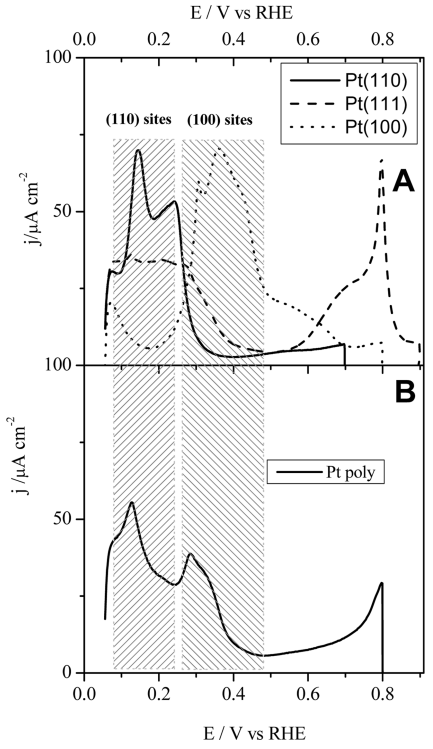

Figure 3. Voltammetric profiles of the Pt basal planes (A) to compare their site distribution with those obtained with a polyoriented platinum electrode (B) in 0.1 M $HClO_4$. Scan rate, 50 mV s^{-1}.

adsorption state, which is the least studied among the platinum single-crystal basal planes.[40−42]

Finally, in this solution, the (111) bidimensional states cannot be identified because they are shifted toward high potentials and overlap with oxygenated species adsorption at (100) and (110) sites, making its identification difficult since no prominent peaks below 0.35 V are associated with this type of sites. As happens in sulfuric acid, (111) sites give a flat contribution in the 0.06−0.30 V region, which cannot be distinguished from those coming from the double-layer charging processes.

Finally, Figure 4 shows the characteristic voltammetric profiles of the different shape-controlled Pt nanoparticles in alkaline medium (0.1 M NaOH). In these voltammetric profiles, the contribution from the gold support has been subtracted in all cases to obtain the "net" voltammetric profile of the nanoparticles. This contribution is important in alkaline media because of the higher amount of OH adsorption on gold in the range between 0.5 and 0.9 V. Figure 5 shows the blank voltammogram of the gold support as well as the blank CV of one of the samples and the resulting CV after subtraction. As previously stated, the main changes occur in the range between 0.5 and 0.9 V, where the gold substrate has significant contributions, with the region below 0.5 V staying almost invariable.

Despite the assumed absence of specific adsorption, the voltammetric profiles also show two well-defined peaks, as in the case of sulfuric acid media, although these peaks appear at higher potentials. The shift toward higher potential values has already been reported for the peaks corresponding to the (110) and (100) steps on the (111) terraces (Figure 6).[43] To identify the different adsorption contributions, Figure 6 shows the voltammetric response of some Pt single-crystal electrodes both

dx.doi.org/10.1021/cs200681x | ACS Catal. 2012, 2, 901−910

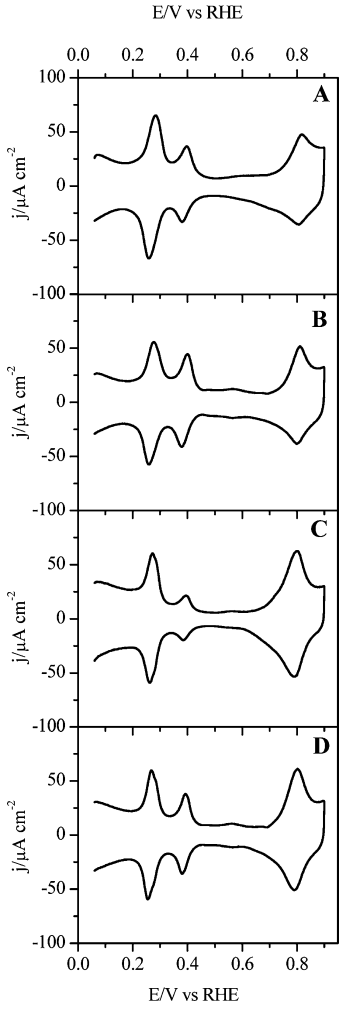

Figure 4. Voltammograms corresponding to (A) $PtNP_{sphe}$, (B) $PtNP_{cubic}$, (C) $PtNP_{tetra}$, and (D) $PtNP_{trunc}$ in 0.1 M NaOH. Scan rate, 50 mV s^{-1}.

basal planes and stepped surfaces, in the same electrolyte. Figure 6A reports the voltammogram of a Pt(111) surface, which shows its characteristic OH adsorption contribution on (111) ordered terraces in the potential range between 0.65 and 0.9 V and a featureless flat signal between 0.06 and 0.3 V. The contributions at high potentials are well-observed in all Pt nanoparticles, but its relative intensity strongly depends on their shape. Thus, the $PtNP_{tetra}$ (Figure 4C) as well as the $PtNP_{trunc}$ (Figure 4D) show a much more intense contribution, in agreement with their expected surface structure, since they contain mostly (111) ordered domains.

On the other hand, the (110) contributions for both the basal planes (Pt(110)) and steps (Pt(610) and Pt(775)) can be delimited in the range between 0.15 and 0.35 V (Figure 6C) with a well-marked peak. Remarkably, for (110) terraces (Figure 6C), a clear shoulder is observed; this shoulder is also present in case of the $PtNP_{tetra}$ (Figure 4C) and $PtNP_{trunc}$ (Figure 4D). The second peak of the voltammograms at ~0.4 V contains the contributions from two different types of sites. As in the case of the peak at 0.27 V for sulfuric acid, it contains the contributions from the (100) sites on the (111) terraces, as shown for the Pt(755) electrode, and also the contributions from the steps on the (100) terraces.[44] As can be seen, this peak is almost absent for the $PtNP_{tetra}$, since the faces of the

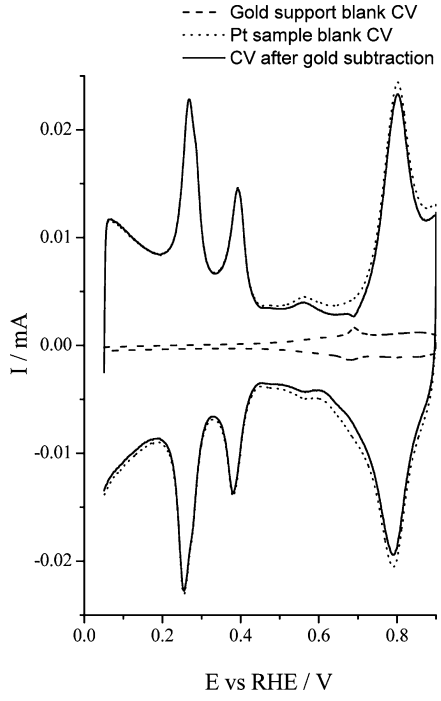

Figure 5. Voltammetric profiles of the gold support (dashed line), $PtNP_{trunc}$ (dotted line), and $PtNP_{trunc}$ after subtraction of the gold contribution (solid line) in 0.1 M NaOH. Scan rate, 50 mV s^{-1}.

nanoparticles have a (111) preferential orientation and the presence of (110) steps and defects on these terraces is favorable with respect to the (100) steps. In addition, the possible rounded edges of the nanoparticles containing (111)

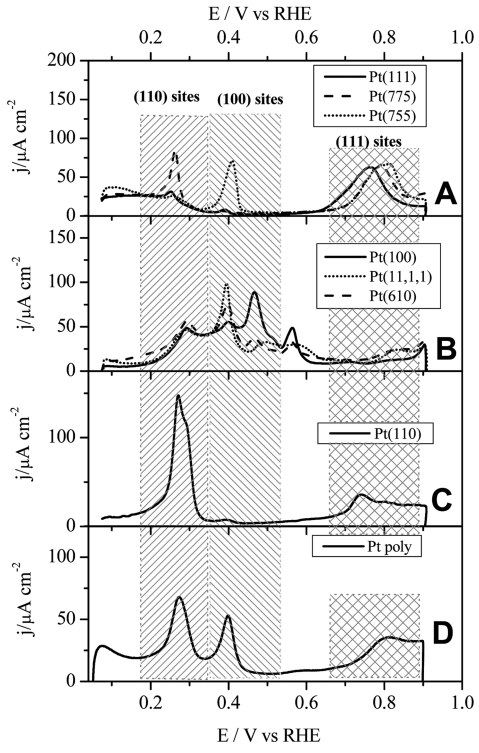

Figure 6. Voltammetric profiles of Pt basal planes and different stepped surfaces (A, B, and C) and a polyoriented platinum electrode (D) in 0.1 M NaOH. Scan rate, 50 mV s^{-1}.

dx.doi.org/10.1021/cs200681x | ACS Catal. 2012, 2, 901–910

faces have a (110) symmetry, which justifies the large intensity of the (110) associated peak and the absence of the (100) step related peak.

The situation is much more complicated for the (100) terrace sites because several adsorption contributions can be observed between 0.2 and 0.65 V for the Pt(100) electrodes.[44−50] However, for a qualitative analysis of the nanoparticles, the characteristic signals coming from (100) terraces can be observed in the potential range between 0.45 and 0.65 V. Interestingly, those Pt nanoparticles with a preferential (100) orientation, as in the case of the $PtNP_{cubic}$ (Figure 4B), as well as those containing some smaller (100) terraces, as in case of the $PtNP_{trunc}$ (Figure 4D), show a broader "double-layer" contribution between 0.45 and 0.65 V, reflecting the preferential orientation of the samples. This feature contrasts with the case of the preferential (111) nanoparticles ($PtNP_{tetra}$) (Figure 4C), which shows a thin "double-layer" contribution, in full agreement with the voltammogram obtained with a Pt (111) single-crystal electrode. The presence of this (100) characteristic voltammetric feature has very important consequences in the determination of the electroactive surface area in this electrolyte and will be discussed in detail in the following section of this paper.

Regarding the nature of the species giving rise to the different peaks, it should be stressed that most of the signals are due to the competitive adsorption/desorption of H/OH, and a clear separation between both processes is not possible. Knowing the adsorbing species on the surface of the supporting electrolyte can be very important to understanding the electrocatalytic activity of the nanoparticles, since the presence of the adsorbed species can catalyze/inhibit the electrochemical process. The measurements of the potential of zero total charge (pztc) can be used to determine the nature of the adsorbed species at the different potentials for surfaces with a well-defined structure. For the Pt(111) electrode, the pztc value lies very close to the so-called double-layer region (0.33 V), and therefore, the contributions below that potential can be unequivocally assigned to hydrogen adsorption processes, whereas the signals between 0.6 and 0.9 V are due to reversible OH adsorption.[43]

Unlike this electrode, the potentials of zero total charge measured for the Pt(100) electrode and the stepped surfaces with (111) and (100) terraces lie in regions where significant currents are measured, revealing that currents in these regions are due to competitive adsorption desorption of OH/H. For the Pt(100) and stepped surfaces with (100) terraces, the pztc values are 0.44−0.46 V for the surfaces with long terraces and 0.39−0.40 V for the surfaces with short terraces.[44] In this case, the value matches that of the peak observed in the voltammograms, which clearly indicates that this peak is due to the competitive adsorption desorption of OH/H. A similar situation is found for the stepped surfaces with (111) terraces and (110) monoatomic steps, for which the pztc coincides with that associated with the (110) sites.[51]

Since the adsorption processes on the nanoparticle are determined by the local environment, that is, the local pztc of the site/domain, three different potential regions can be defined. Above 0.6 V, the signal is mainly due to the adsorption of OH on the (111) ordered domains and probably some incipient oxidation/adsorption of OH of the rest of the sites. For that reason, this region can be unequivocally assigned to OH adsorption. Below 0.2 V, all the signals can be assigned to hydrogen adsorption/desorption processes, since this potential is well below the local pztc of the different sites. The intermediate region (0.2−0.6 V) should be assigned to the competitive adsorption/desorption processes of OH on the surface sites. It should be stressed that this situation is clearly observed in the main peaks.

The results shown up to now clearly indicate that the voltammetric features obtained with different shape-controlled clean Pt nanoparticles (Figure 4) perfectly correlate with those obtained with Pt single-crystal electrodes (Figure 6). In addition, we have found a good correlation between their characteristic shapes, estimated by ex-situ TEM measurement, and their preferential surface structures, which points out that the indispensable/required manipulation of the samples from the as-prepared colloidal suspension to the "cleaned" water suspension, as well as the final electrochemical cleaning step involving a simple CO adsorption and stripping, does not significantly modify the platinum surface order of the nanoparticles. This fact contrasts with our previous finding in which we evidenced that the UV/ozone irradiation cleaning of shape-controlled Pt nanoparticles remarkably altered their atomic surface structure, thus significantly modifying their electrocatalytic properties.[52]

Determination of the Electrochemical Active Surface Area in Alkaline Medium. The determination of the active area of electrocatalysts is essential, first of all, to compare the performance of the different electrocatalysts and, second, to prove any enhancement in this performance. Traditionally, the determination of the active area of platinum has been assessed using the charge measured under the adsorption states at low potentials (the so-called hydrogen adsorption region) for an electrode of known active area. Thus, a reference value for the charge density for this region is obtained, and this value can be used to determine the active area of any electrode whose area cannot be measured directly by physical methods.

The first reference values for the charge density were obtained for electrochemically cycled polycrystalline samples with no preferential orientation.[53] However, these values could not be appropriate for surfaces with preferential orientations. For instance, surfaces with a large fraction of (111) domains or (100) domains have contributions from these sites at potentials in which the typical polycrystalline platinum has no contributions, as can be seen in Figure 1. Recently, the reference values for charge density for platinum electrodes in perchloric and sulfuric acid media have been revisited and reformulated to take into account the possible presence of preferential orientations.[10] As a brief summary, the charge density measured for the region between 0.06 and 0.6 V, after subtraction of the apparent double-layer stands for 230 $\mu C\ cm^{-2}$ in sulfuric acid solutions, whereas in perchloric acid, solution the reference value is 200 $\mu C\ cm^{-2}$.

For alkaline solutions, the reported reference value is 145 $\mu C\ cm^{-2}$ for the charge measured between 0.06 and 0.45 V after the subtraction of the apparent double layer, a significantly lower value than that used in acidic media. In the case of sulfuric or perchloric acid, there is a potential region in which there are no significant contributions from adsorbed species so that an apparent double layer can be easily determined. Moreover, in the case of sulfuric acid solutions, no contributions are observed between 0.6 and 0.8 V for any single crystal (see Supporting Information Figure S4) so that this region can be used to establish the double layer. For alkaline medium, there is no such region where significant adsorption processes are absent. For instance, the Pt(111) and stepped surfaces with (111) terraces have a double-layer region

dx.doi.org/10.1021/cs200681x | ACS Catal. 2012, 2, 901−910

between 0.45 and 0.6 V. However, large current densities are observed in this region for the surfaces having (100) terrace domains. These distinct contributions can be observed for the different nanoparticles (although to a different extent) so that a clear double layer is not observed. This is especially the case for $PtNP_{cubic}$, for which the apparent double layer between 0.4 and 0.6 V is larger than in the other cases due to the presence in this region of the adsorption states corresponding to large (100) domains.

To determine whether the classical approach was valid for the nanoparticles, the voltammograms for the different samples were recorded initially in sulfuric acid and then immediately transferred to 0.1 M NaOH to record a second voltammogram. The area determined in sulfuric acid is then compared with that estimated in alkaline medium by subtracting the apparent double layer measured between 0.45 and 0.46 V (the potential at which the minimum current is measured) and using a reference value of 145 μC cm^{-2}. The determined values from alkaline medium are significantly different from those in sulfuric acid, ranging from a −12% difference for the $PtNP_{cubic}$ to an 8% for the $PtNP_{tetra}$.

These differences clearly arise from the selection of the double layer. For the $PtNP_{cubic}$, at 0.45 V, the current has a significant contribution from the (100) sites so that the active area is underestimated. On the other hand, the area is overestimated for the (111) nanoparticles, which have the lowest ratio of (100) sites, lower than the typical polycrystalline sample. These differences mean that the pure double-layer contributions cannot be determined in the samples, and a different approach for measuring the active area should be used. For the single-crystal electrodes, the total voltammetric charge measured between 0.06 and 0.90 V (without any double-layer correction) is very similar for all the electrodes. It should be stressed that in this potential region, the only processes taking place are the hydrogen and OH reversible adsorption. The charges in this region range from 350 μC cm^{-2} for the (111) electrode to 410 μC cm^{-2} for several stepped and kinked surfaces. In fact, the charge values for kinked surfaces have total charge density values between 380 and 400 μC cm^{-2}. Because of the small difference in the total charge for the different stepped and kinked surfaces, this value can be used tentatively to calculate the active area in alkaline medium. Thus, a reference value for the total charge measured between 0.06 and 0.90 V (without subtraction of double layer) of 390 μC cm^{-2} was chosen, and the areas determined using this method were compared with those in sulfuric acid. The differences between both measurements were always below ±1.5%, which is below the typical error in this determination. Thus, the new method for measuring the active area in NaOH solutions can be considered equivalent to that established for sulfuric acid solutions, allowing a direct comparison of the current densities measured in both media.

Table 1 summarizes the electroactive surface area results obtained. In addition, for sake of comparison, the surface area estimated from the CO stripping charge in NaOH and using a charge density value of 420 μC cm^{-2}, is also included. As can be observed, the differences between the areas calculated from the CO stripping charges and those previously obtained are now much higher, mainly as a result of the dependence of the CO coverage on the surface orientation and also the uncertainties of the baseline correction. In addition, very recently, Chen et al. also concluded that, among various methods (i.e., the adsorption/stripping of adsorbed probe species, such as hydrogen (H), copper (Cu), and carbon monoxide (CO), oxygen and hydroxide (O/OH), and potentiostatic CO/H displacement as well as double-layer capacitance to evaluate the electrochemically active surface areas (ECAs) of a large variety of platinum electrodes), the CO stripping method was not appropriate for the determination of an ECA of rough film nano-Pt with high dispersion, since adsorbed CO molecules caused a significant annealing effect (more than 20% decrease in ECAs after four consecutive times of adsorption and stripping).[54]

Table 1. Comparison of the Active Surface Area Values Obtained for the Different Shape-Controlled Pt Nanoparticles and for a Polycrystalline Pt Electrode

	NaOH/ cm^2	H_2SO_4/ cm^2	relative error/%	CO_{strip} in NaOH/cm^2	relative error/%
$PtNP_{sphe}$	0.726	0.717	+1.3	0.677	−5.5
$PtNP_{cubic}$	0.565	0.570	−0.9	0.555	−2.7
$PtNP_{tetra}$	0.166	0.164	+1.3	0.158	−3.8
$PtNP_{trunc}$	0.385	0.380	+1.1	0.332	−12.7
Poly Pt	0.195	0.193	+1.0	0.205	+6.4

CO Stripping at Shape-Controlled Pt Nanoparticles in Alkaline Medium. CO oxidation on platinum electrodes in alkaline medium exhibits some characteristics that clearly differentiate its behavior from that observed in acidic solutions. In acidic media, essentially a single stripping peak is observed on the different single-crystal surfaces, independently of the symmetry of the terrace or the presence of steps. On the other hand, CO oxidation on stepped and kinked surfaces with (111) terraces in alkaline solution gives rise to several peaks associated with the different sites of the surface. Thus, the CO stripping voltammogram on kinked surfaces with (111) terraces exhibits three different peaks at 0.59, 0.70, and 0.78 V, which correspond to the oxidation of CO on the (110) step (kink) sites, on the (100) step (kink) sites, and (111) terrace sites, respectively.[18,20−22] It has been proposed that the multiple peaks are due to the low mobility of CO on the (111) terraces.[18,22] On the other hand, only one peak is observed for the stepped surfaces with (100) terraces, which suggests a faster mobility of CO on that type of domain.[44] In this latter case, the presence of steps catalyzes the oxidation of CO because the peak shifts toward lower potential values as the step density increases. For the stepped surfaces with (100) terraces, the peak appears between 0.62 and 0.67 V. In addition, a significant prewave at ∼0.50 V is observed for all the surfaces, which has been associated with the oxidation of compressed CO adlayers.[18,22,55,56]

This complex dependence of the CO oxidation behavior in alkaline medium on the surface structure also affects the behavior of the polycrystalline electrode. As shown in Figure 7, the CO stripping voltammogram shows a prepeak and multiple oxidation peaks, which can be associated with the different surface sites present on the electrode. Aside from the initial prewave, the broad contribution from 0.52 to 0.60 V contains multiple peaks not well resolved, as can be recognized from its irregular shape. These contributions are probably coming from zero- and one-dimensional domains (defects, steps, and kinks), but owing to the heterogeneous nature of the surface, it cannot be easily assigned to the different sites on the surface. When compared with the situation observed in acid solutions, the peak is shifted ∼100 mV toward lower potentials with respect to that measured in sulfuric acid solutions, a clear indication of

dx.doi.org/10.1021/cs200681x | ACS Catal. 2012, 2, 901−910

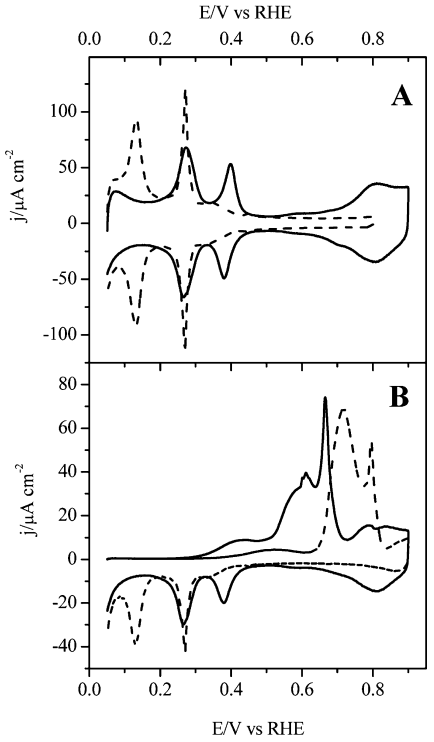

Figure 7. (A) Voltammetric profiles of a polycrystalline electrode in 0.1 M NaOH (full line) and 0.5 M H_2SO_4 (dashed line) (scan rate, 50 mV s^{-1}). (B) CO stripping voltammograms in 0.1 M NaOH (full line) and 0.5 M H_2SO_4 (dashed line) (scan rate, 20 mV s^{-1}).

the higher activity for CO oxidation of platinum in this medium. In addition, the two peaks in sulfuric acid solutions are linked to the short- and long-range ordered domains of the polycrystalline electrode, as has been determined by the comparison between stepped surfaces and preferentially polyoriented nanoparticles.[28]

When the CO oxidation reaction is studied on the nanoparticles (Figure 8), different behaviors can be observed for the different nanoparticles. Some of them can be directly related to the observed behavior of the single-crystal electrodes. The behavior of the $PtNP_{sphe}$ is very similar to that observed for the polycrystalline electrode (Figure 7B). A broad contribution

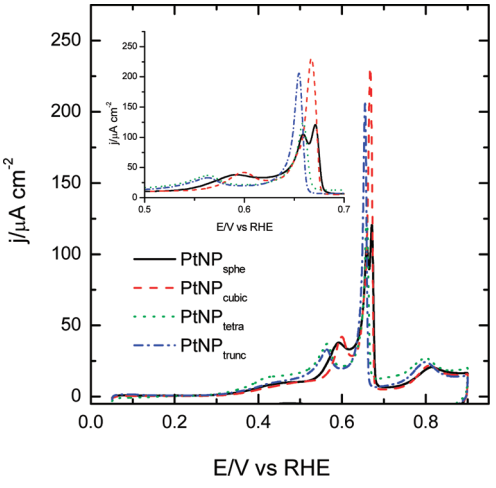

Figure 8. CO stripping voltammogram in 0.1 M NaOH for $PtNP_{sphe}$, $PtNP_{cubic}$, $PtNP_{tetra}$, and $PtNP_{trunc}$. Scan rate, 20 mV s^{-1}.

between 0.52 and 0.60 V is observed with the main peak at 0.67 V. The major difference is that the charge for the main peak is larger in the case of the nanoparticles, probably related to a slightly different distribution of the sites in the two electrodes. In this respect, the profiles for both hydrogen adsorption in the low potential range and OH adsorption above this electrode potential are slightly different, which probably affects CO oxidation. It should be stressed that, for this medium, no significant agglomeration effects in the CO stripping peaks have been found. Unlike the observed behavior of the spherical nanoparticles in acid media,[57] the CO stripping peak potentials for samples dispersed on carbon in which the nanoparticles are isolated are almost identical to those reported in Figure 7.

For the $PtNP_{cubic}$ sample, the expected behavior would be a single peak around 0.62−0.67 V, as observed for the stepped surfaces with narrow (100) terraces. In fact, this peak is observed at 0.67 V, which indicates that the mean size of the ordered domains is relatively small.[44] In addition, there is a peak at 0.60 V that can be assigned to the presence of zero- and one-dimensional order domains, as in the case of the polycrystalline electrode.

A completely different case is that of the $PtNP_{tetra}$ and $PtNP_{trunc}$ electrodes. If the behavior of the stepped and kinked surfaces with (111) terraces could be directly extrapolated to the $PtNP_{tetra}$,[18] a significant contribution would be expected at ~0.57 V, linked to the presence of (110) defect sites on (111) terraces and other minor contributions at higher potentials linked to the (100) defects (whose peak at 0.4 V in the blank voltammogram is almost absent) and (111) terraces. The contribution at 0.57 V is present, but the main peak is observed at 0.65 V, which has not been observed for any stepped or kinked surface with (111) terraces. A very similar situation is observed for the $PtNP_{trunc}$. Thus, this additional peak has to be related either to sites present in the nanoparticles at a significant ratio and absent from stepped and kinked surfaces (i.e., edge sites[58]) or to a modified reactivity of the nanoparticles with (111) domains.

To study the role of the defects and edge sites on the CO oxidation mechanism, submonolayer coverages of bismuth were deposited on the nanoparticles, and CO oxidation was studied on those modified nanoparticles. Bismuth deposition on stepped surfaces with (111) terraces and tetrahedral nanoparticles is a stepwise nanoparticle process in which the deposition takes place initially on the steps and defect sites and only when these sites have been covered deposition process continues on the terrace.[58,59] In addition, Bi on the (111) terrace shows a characteristic redox peak at 0.625 V.[60] Two different Bi coverages on the nanoparticles have been studied (inset of Figure 9). In the first one, (110) and (100) defect sites have been partially covered, but no Bi has yet been deposited on the (111) domains, since the characteristic peak for bismuth on the (111) terraces is absent. In the second one, there is already some Bi on the terraces, and all the (110) and (100) sites have been covered. The CO stripping voltammograms in alkaline medium for those electrodes are shown in Figure 9.

Several changes can be noticed in the stripping voltammograms as compared with that obtained for the unmodified nanoparticles: First, stripping peaks shift toward positive potentials, in a way that is similar to that found in acid media.[58] Second, the peak at lower potential completely disappears when all the (110) sites have been covered, confirming the relationship between these peaks and the (110) sites. Third, the peak at 0.65 V moves toward positive

dx.doi.org/10.1021/cs200681x | ACS Catal. 2012, 2, 901−910

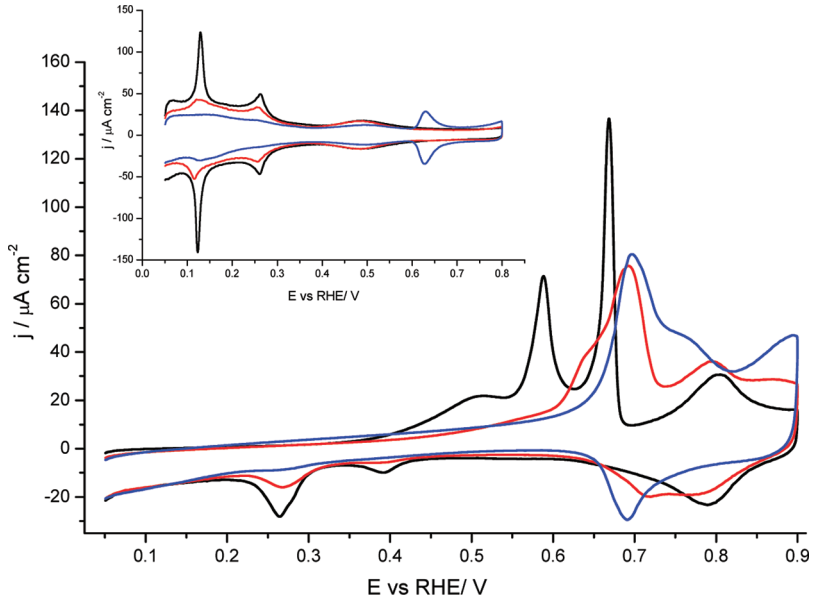

Figure 9. CO stripping voltammogram in 0.1 M NaOH for $PtNP_{tetra}$ modified with Bi adatoms. Scan rate, 20 mV s^{-1}. Inset: voltammograms corresponding to $PtNP_{tetra}$ modified with Bi adatoms in 0.5 M H_2SO_4. Scan rate, 50 mV s^{-1}.

potential values and becomes wider with the additional appearance of a shoulder when (110) and (100) sites have been completely blocked. In this situation, only (111) ordered domains are not blocked on the surface. As has been already proposed, these decorated $PtNP_{tetra}$ electrodes have relatively wide (111) domains and also isolated sites which could adsorb solely hydrogen. Since the only observed CO stripping peak in this situation is that at 0.70 V, which corresponds to that observed at 0.65 V, this peak should be related to the stripping of CO that was initially adsorbed on the (111) ordered domains. The reason why the reactivity of these domains is higher than that observed for the (111) terraces is still not clear. To understand such changes in the reactivity, more work is under progress. For the $PtNP_{trunc}$ electrodes, the situation is very similar to that described for the $PtNP_{tetra}$. For this sample, the only difference with respect to the observed behavior of the $PtNP_{tetra}$ is the relative intensities of the different peaks.

CONCLUSIONS

The analysis of the results in the different media demonstrates that the voltammetric profile of the platinum nanoparticles in sulfuric acid, perchloric acid, and alkaline media can be used as a characterization tool of the surface structure of the nanoparticles. Although the surface structure of the nanoparticles is always much more complex than that of the platinum single crystals, a good correlation between the voltammograms and the average shape of the nanoparticles determined by TEM is obtained. The characteristic peaks can be employed to determine whether the nanoparticles have been cleaned from the surfactants used during the synthetic procedures. In addition, for the nanoparticle characterization and determination of the electrocatalytic activity, an accurate determination of the active area of the electrocatalysts is very important. For that reason, a new criterion for estimating the active surface area of the nanoparticles in alkaline medium has been established. For this medium, the total charge measured between 0.06 and 0.90 V (without any double-layer correction) stands for 390 μC cm^{-2}. The areas determined with this method are in perfect agreement with those measured in acidic media. For CO oxidation experiments, it has been found that the behavior of the nanoparticles having a large fraction of (111) ordered domains deviates from that expected from the single-crystal electrodes with (111) terraces. For the rest of the nanoparticles, the CO stripping voltammogram agrees with that of the corresponding single-crystal electrodes.

ASSOCIATED CONTENT

Supporting Information

Detailed experimental procedure for the synthesis of the nanoparticles, together with data from the TEM characterization and the quantification of the different surface sites obtained from the irreversible adsorption of Ge and Bi. This material is available free of charge via the Internet at http://pubs.acs.org.

AUTHOR INFORMATION

Corresponding Author

*E-mails: (E.H.) herrero@ua.es; (J.M.F.) juan.feliu@ua.es.

Notes

The authors declare no competing financial interest.

ACKNOWLEDGMENTS

This work has been financially supported by the MICINN (Spain) (Project CTQ2010-16271) and Generalitat Valenciana (Project PROMETEO/2009/045, -FEDER).

REFERENCES

(1) Markovic, N. M.; Gasteiger, H. A.; Ross, P. N. *J. Phys. Chem.* **1995**, *99*, 3411−3415.

(2) Maciá, M. D.; Campina, J. M.; Herrero, E.; Feliu, J. M. *J. Electroanal. Chem.* **2004**, *564*, 141−150.

(3) Kuzume, A.; Herrero, E.; Feliu, J. M. *J. Electroanal. Chem.* **2007**, *599*, 333−343.

(4) Koper, M. T. M.; Lai, S. C. S.; Herrero, E., Mechanisms of the Oxidation of Carbon Monoxide and Small Organic Molecules at Metal Electrodes. In *Fuel Cell Catalysis, A Surface Science Approach*; Koper, M. T. M., Ed.; John Wiley & Sons, Inc: Hoboken, NJ, 2009; pp 159−208.

(5) Vidal-Iglesias, F. J.; Solla-Gullón, J.; Rodríguez, P.; Herrero, E.; Montiel, V.; Feliu, J. M.; Aldaz, A. *Electrochem. Commun.* **2004**, *6*, 1080−1084.
(6) Solla-Gullon, J.; Vidal-Iglesias, F. J.; Feliu, J. M. *Annu. Rep. Prog. Chem., Sect. C: Phys. Chem.* **2011**, *107*, 263−297.
(7) Koper, M. T. M. *Nanoscale* **2011**, *3*, 2054−2073.
(8) Lee, I.; Delbecq, F.; Morales, R.; Albiter, M. A.; Zaera, F. *Nat. Mater.* **2009**, *8*, 132−138.
(9) Sanchez-Sanchez, C. M.; Solla-Gullon, J.; Vidal-Iglesias, F. J.; Aldaz, A.; Montiel, V.; Herrero, E. *J. Am. Chem. Soc.* **2010**, *132*, 5622−5624.
(10) Chen, Q. S.; Solla-Gullon, J.; Sun, S. G.; Feliu, J. M. *Electrochim. Acta* **2010**, *55*, 7982−7994.
(11) Clavilier, J. Flame-Annealing and Cleaning Technique. In *Interfacial Electrochemistry*; Wieckowski, A., Ed.; Marcel Dekker, Inc.: New York, 1999; pp 231−248.
(12) Rodes, A.; Elachi, K.; Zamakhchari, M. A.; Clavilier, J. *J. Electroanal. Chem.* **1990**, *284*, 245−253.
(13) Clavilier, J.; Elachi, K.; Rodes, A. *J. Electroanal. Chem.* **1989**, *272*, 253−261.
(14) Parsons, R.; Ritzoulis, G. *J. Electroanal. Chem.* **1991**, *318*, 1−24.
(15) Furuya, N.; Koide, S. *Surf. Sci.* **1989**, *220*, 18−28.
(16) Clavilier, J. *ACS Symp. Ser.* **1988**, *378*, 202−215.
(17) Clavilier, J.; Elachi, K.; Rodes, A. *Chem. Phys.* **1990**, *141*, 1−14.
(18) Herrero, E.; Chen, Q.-S.; Hernandez, J.; Sun, S.-G.; Feliu, J. M. *Phys. Chem. Chem. Phys.* **2011**, *13*, 16762−16771.
(19) García, G.; Koper, M. T. M. *ChemPhysChem* **2011**, *12*, 2064−2072.
(20) Garcia, G.; Koper, M. T. M. *J. Am. Chem. Soc.* **2009**, *131*, 5384−5385.
(21) Garcia, G.; Koper, M. T. M. *Phys. Chem. Chem. Phys.* **2009**, *11*, 11437−11446.
(22) Garcia, G.; Koper, M. T. M. *Phys. Chem. Chem. Phys.* **2008**, *10*, 3802−3811.
(23) Solla-Gullón, J.; Montiel, V.; Aldaz, A.; Clavilier, J. *J. Electrochem. Soc.* **2003**, *150*, E104−E109.
(24) Solla-Gullón, J.; Rodríguez, P.; Herrero, E.; Aldaz, A.; Feliu, J. M. *Phys. Chem. Chem. Phys.* **2008**, *10*, 1359−1373.
(25) Solla-Gullón, J.; Vidal-Iglesias, F. J.; López-Cudero, A.; Garnier, E.; Feliu, J. M.; Aldaz, A. *Phys. Chem. Chem. Phys.* **2008**, *10*, 3689−3698.
(26) Vidal-Iglesias, F. J.; Solla-Gullon, J.; Perez, J. M.; Aldaz, A. *Electrochem. Commun.* **2006**, *8*, 102−106.
(27) Ahmadi, T. S.; Wang, Z. L.; Green, T. C.; Henglein, A.; El-Sayed, M. A. *Science* **1996**, *272*, 1924−1926.
(28) Solla-Gullón, J.; Vidal-Iglesias, F. J.; Herrero, E.; Feliu, J. M.; Aldaz, A. *Electrochem. Commun.* **2006**, *8*, 189−194.
(29) Clavilier, J.; Armand, D.; Sun, S. G.; Petit, M. *J. Electroanal. Chem.* **1986**, *205*, 267−277.
(30) Rodes, A.; Zamakhchari, M. A.; Elachi, K.; Clavilier, J. *J. Electroanal. Chem.* **1991**, *305*, 115−129.
(31) Al-Akl, A.; Attard, G.; Price, R.; Timothy, B. *Phys. Chem. Chem. Phys.* **2001**, *3*, 3261−3268.
(32) Rodríguez, P.; Herrero, E.; Solla-Gullón, J.; Vidal-Iglesias, F. J.; Aldaz, A.; Feliu, J. M. *Electrochim. Acta* **2005**, *50*, 4308−4317.
(33) Rodríguez, P.; Solla-Gullón, J.; Vidal-Iglesias, F. J.; Herrero, E.; Aldaz, A.; Feliu, J. M. *Anal. Chem.* **2005**, *77*, 5317−5323.
(34) Solla-Gullón, J.; Vidal-Iglesias, F. J.; Rodríguez, P.; Herrero, E.; Feliu, J. M.; Clavilier, J.; Aldaz, A. *J. Phys. Chem. B* **2004**, *108*, 13573−13575.
(35) Rodríguez, P.; Herrero, E.; Solla-Gullón, J.; Vidal-Iglesias, E. J.; Aldaz, A.; Feliu, J. M. *Electrochim. Acta* **2005**, *50*, 3111−3121.
(36) Rodríguez, P.; Herrero, E.; Aldaz, A.; Feliu, J. M. *Langmuir* **2006**, *22*, 10329−10337.
(37) Gómez, R.; Orts, J. M.; Alvarez-Ruiz, B.; Feliu, J. M. *J. Phys. Chem. B* **2004**, *108*, 228−238.
(38) Climent, V.; Gómez, R.; Orts, J. M.; Feliu, J. M. *J. Phys. Chem. B* **2006**, *110*, 11344−11351.
(39) Wakisaka, M.; Udagawa, Y.; Suzuki, H.; Uchida, H.; Watanabe, M. *Energy Environ. Sci.* **2011**, *4*, 1662−1666.
(40) Kibler, L. A.; Cuesta, A.; Kleinert, M.; Kolb, D. M. *J. Electroanal. Chem.* **2000**, *484*, 73−82.
(41) Gómez, R.; Clavilier, J. *J. Electroanal. Chem.* **1993**, *354*, 189−208.
(42) Souza-Garcia, J.; Climent, V.; Feliu, J. M. *Electrochem. Commun.* **2009**, *11*, 1515−1518.
(43) Climent, V.; Gómez, R.; Orts, J. M.; Aldaz, A.; Feliu, J. M. *Potential of Zero Total Charge of Platinum Single Crystal Electrodes*. The Electrochemical Society, Inc.: Pennington, NJ, 2000; Vol. *2000−16*; pp 12−30.
(44) Arán-Ais, R. M.; Figueiredo, M. C.; Vidal-Iglesias, F. J.; Climent, V.; Herrero, E.; Feliu, J. M. *Electrochim. Acta* **2011**, *58*, 184−192.
(45) Vidal-Iglesias, F. J.; Solla-Gullón, J.; Montiel, V.; Feliu, J. M.; Aldaz, A. *J. Phys. Chem. B* **2005**, *109*, 12914−12919.
(46) Vidal-Iglesias, F. J.; Garcia-Araez, N.; Montiel, V.; Feliu, J. M.; Aldaz, A. *Electrochem. Commun.* **2003**, *5*, 22−26.
(47) Schmidt, T. J.; Ross, P. N.; Markovic, N. M. *J. Phys. Chem. B* **2001**, *105*, 12082−12086.
(48) Markovic, N. M.; Gasteiger, H. A.; Philip, N. *J. Phys. Chem. B* **1996**, *100*, 6715−6721.
(49) Rodes, A.; Climent, V.; Orts, J. M.; Pérez, J. M.; Aldaz, A. *Electrochim. Acta* **1998**, *44*, 1077−1090.
(50) van der Vliet, D. F.; Koper, M. T. M. *Surf. Sci.* **2010**, *604*, 1912−1918.
(51) Unpublished results.
(52) Vidal-Iglesias, F. J.; Solla-Gullón, J.; Herrero, E.; Montiel, V.; Aldaz, A.; Feliu, J. M. *Electrochem. Commun.* **2011**, *13*, 502−505.
(53) Trasatti, S.; Petrii, O. A. *Pure Appl. Chem.* **1991**, *63*, 711−734.
(54) Chen, D.; Tao, Q.; Liao, L. W.; Liu, S. X.; Chen, Y. X.; Ye, S. *Electrocatalysis* **2011**, *2*, 207−219.
(55) Markovic, N. M.; Ross, P. N. *Surf. Sci. Rep.* **2002**, *45*, 121−229.
(56) Spendelow, J. S.; Goodpaster, J. D.; Kenis, P. J. A.; Wieckowski, A. *J. Phys. Chem. B* **2006**, *110*, 9545−9555.
(57) López-Cudero, A.; Solla-Gullón, J.; Herrero, E.; Aldaz, A.; Feliu, J. M. *J. Electroanal. Chem.* **2010**, *644*, 117−126.
(58) Chen, Q. S.; Vidal-Iglesias, F. J.; Solla-Gullón, J.; Sun, S. G.; Feliu, J. M. *Chem. Sci.* **2012**, *3*, 136−147.
(59) Herrero, E.; Climent, V.; Feliu, J. M. *Electrochem. Commun.* **2000**, *2*, 636−640.
(60) Clavilier, J.; Feliu, J. M.; Aldaz, A. *J. Electroanal. Chem.* **1988**, *243*, 419−433.